AGU ADVANCING EARTH AND SPACE SCIENCE

JGR Space Physics

METHOD

10.1029/2022JA030724

Special Section:
Fifteen Years of THEMIS Mission

Comparison of Energetic Electron Fluxes Measured by GPS and THEMIS Spacecraft in the Inner Magnetosphere

Reed Curtis[1], Anton V. Artemyev[2], Dmitri L. Vainchtein[1], Adam Kellerman[2], Steven K. Morley[3], and Vassilis Angelopoulos[2]

[1]Nyheim Plasma Institute, Drexel University, Camden, NJ, USA, [2]Earth, Planetary, and Space Sciences, University of California, Los Angeles, CA, USA, [3]Space Science and Applications, Los Alamos National Laboratory, Los Alamos, NM, USA

Key Points:

- Energetic electron fluxes measured by THEMIS have been compared to fluxes measured by GPS satellites
- Ratio of GPS and THEMIS fluxes for energies 100–600 keV has been fitted as a function of *L*-shell
- Projected GPS fluxes allows tracing the electron flux *L*-shell distributions with <1 hr time resolution

Supporting Information:

Supporting Information may be found in the online version of this article.

Correspondence to:

R. Curtis,
rac364@drexel.edu

Citation:

Curtis, R., Artemyev, A. V., Vainchtein, D. L., Kellerman, A., Morley, S. K., & Angelopoulos, V. (2022). Comparison of energetic electron fluxes measured by GPS and THEMIS spacecraft in the inner magnetosphere. *Journal of Geophysical Research: Space Physics*, *127*, e2022JA030724. https://doi.org/10.1029/2022JA030724

Received 6 JUN 2022
Accepted 9 SEP 2022

Abstract Key elements of space weather models are energetic electron fluxes in the inner magnetosphere and the outer radiation belt. Flux depletion is driven by various loss processes: scattering into atmosphere, magnetopause shadowing. Flux enhancement is driven by various acceleration processes: local wave-particle interactions, radial transport, plasma sheet injections. Many of these processes operate on ∼ hour timescales. Such mesoscale flux variations are not well traced by equatorial spacecraft with much longer orbits. Energetic electron detectors onboard the Global Positioning System (GPS) constellation provide a unique opportunity for probing such ∼ hour-scale flux variations. Measurements from up to 23 identically instrumented GPS satellites cover a wide energy and *L*-shell range with a subhour time resolution. However, their orbits are inclined and thus all measurements at *L*-shell >4.3 are off-equatorial. In this report, we present a comparison of equatorial THEMIS and nonequatorial GPS measurements of omnidirectional ≤600 keV electron fluxes. Such a comparison allows us to derive coefficients for using off-equatorial GPS fluxes to infer the equatorial values. These coefficients depend on particle energy and *L*-shell. We demonstrate a new data set derived from GPS measurements and discuss how it can be used to investigate mesoscale dynamics of energetic electron fluxes in the inner magnetosphere.

1. Introduction

Dynamics of energetic electron fluxes in the outer radiation belt are controlled by a balance between electron losses and acceleration (Millan & Baker, 2012; Millan & Thorne, 2007). There are many mechanisms contributing to both processes (see reviews by Shprits, Subbotin, Meredith, & Elkington (2008), Shprits, Elkington, Meredith, Subbotin (2008), Li & Hudson (2019), and Thorne et al. (2021)). Initially transported from the plasma sheet, electrons undergo the adiabatic acceleration (Galperin et al., 1978; Lyons, 1984), which is especially effective for fast spatially localized injections (Birn et al., 1998, 2004; Gabriels et al., 2012, 2014) occurring on the timescale of minutes to about an hour (Gabrielse et al., 2019; Sorathia et al., 2018; Turner et al., 2016). The injected electron populations are quite unstable to the generation of whistler-mode waves (Le Contel et al., 2009; Tao et al., 2011; X. Zhang, Angelopoulos, et al., 2018), that further accelerate a small fraction of injected electrons (Chen et al., 2007; Green & Kivelson, 2004). Such an acceleration is generally a diffusive process (Horne et al., 2005; Shprits, Subbotin, Meredith, & Elkington, 2008), that results in formation of relativistic electron fluxes on a timescale of hours (Allison & Shprits, 2020; Li, Thorne, et al., 2014; Thorne et al., 2013). However, a much faster electron acceleration is possible within spatially localized sources regions of intense whistler-mode waves (Agapitov et al., 2015; Foster et al., 2014; Gan et al., 2020). Electron loss mechanisms include the electron scattering by waves (Millan & Thorne, 2007) and losses through the magnetopause (Hudson et al., 2014; Shprits et al., 2006; Turner et al., 2012). Depending on the wave-mode contributing to scattering, electron losses can take from days (e.g., for electron scattering by low-intensity hiss waves, see Ma et al., 2016, 2017; Mourenas et al., 2017; Ni et al., 2013) to minutes (e.g., for electron scattering by electromagnetic ion cyclotron waves, see Blum, Li, & Denton, 2015; Grach et al., 2021; Kersten et al., 2014; Ni et al., 2015; Omura & Zhao, 2013). Overall, the range of timescales of losses through the magnetopause is quite large, are similar to a large range of the magnetopause motion scales controlled by solar wind transients (Elkington et al., 2004; Hudson et al., 1999, 2008). All these mechanisms of electron acceleration and losses cause electron flux variations on timescales from minutes to days (Claudepierre et al., 2020a, 2020b; Morley, Friedel, Cayton, et al., 2010; Turner et al., 2013, 2015).

Spacecraft probing and tracing of electron fluxes at different timescales is crucial for quantifying relative contributions of different acceleration and loss mechanisms. There are two main approaches for such tracing. (a) Equatorial spacecraft observe the evolution of electron fluxes within a certain L-shell range with time steps of about spacecraft orbit period. This time step is reduced for multispacecraft missions (e.g., THEMIS and Van Allen Probes; see Thorne et al. (2013); Turner et al. (2013); Shprits et al. (2016)) for particular events, but still mostly remains about several hours (Claudepierre et al., 2020a, 2020b; Turner et al., 2015). (b) Low-altitude spacecraft yield electron flux L-shell profiles collected every few minutes, and the time step between such snapshot-profiles is about couple of hours for typical spacecraft orbit periods (e.g., POES, see Capannolo et al., 2018, 2019, CubeSats, e.g., Mourenas et al., 2021; Zhang, Li, et al., 2017 and others Y. Zhang, Ni, et al., 2018). However, low-altitude measurements are restricted to a relatively small fraction of the equatorial electron distribution around and within the loss cone pitch angles. Evolution of this low pitch angle electron distribution does not necessary reflect the evolution of the core population trapped around the equator, and such measurements are mostly useful during strong-scattering events characterizing by nearly isotropic equatorial electron distributions (see discussion in Rodger et al. (2013)).

A promising opportunity for tracing the electron flux dynamics with a sufficiently high time resolution using measurements of multiple Global Positioning System (GPS) satellites has been demonstrated by Morley, Friedel, Clayton, et al. (2010); Morley et al. (2016), Boynton et al. (2017), and Smirnov et al. (2020). Up to 23 satellites (in the v1.09 public release of GPS particle data, see Carver et al., 2020; Niyazov et al., 2021) travel along medium Earth orbits (with the equator crossing around $L \sim 4.2$) and are equipped with Combined X-ray Dosimeter (Morley et al., 2016; Morley, Friedel, Spanswick, et al., 2010). Combining measurements of identical detectors on multiple satellites, one can obtain a continuous (L-shell, time) distribution of electron fluxes with a sufficiently small time step $\leq$1 hr. GPS orbits, however, allow equatorial flux measurements only at $L \sim 4.2$, whereas measurements at high L-shells gather only a fraction of the equatorial electron population with pitch angles sufficiently small to reach middle latitudes of GPSs. Therefore, to estimate (L-shell, time) distributions of equatorial electron fluxes for a wide L-shell range, the GPS measurements should be projected to estimate the equatorial flux. In this report, we provide the formulas for such a projection based on comparison of conjugated GPS and equatorial THEMIS observations. Such projection technique is similar to techniques previously proposed for comparison of near-equatorial measurements with measurements of low-orbiting spacecraft (Allison et al., 2018; Claudepierre & O'Brien, 2020).

This paper has the following structure: the description of GPS and THEMIS conjunction measurements is in Sect. 2, estimations of the projection factors for different GPS energy channels, L-shells is in Section 3, verification of projected GPS measurements is in Section 4, discussion of an applicability of a new data set derived from GPS for resolving equatorial electron flux dynamics is in Section 5. Finally, conclusions are in Section 6.

2. GPS and THEMIS Data Sets

To compare GPS and THEMIS (Angelopoulos, 2008) energetic electron fluxes, we collect the statistics of events with conjunctions of one of three THEMIS spacecraft (ThA, ThD, ThE) and one of GPS spacecraft (#53–73, excluding #60). Each event includes 4 min measurement of GPS Combined X-ray Dosimeter (CXD) (Distel et al., 1999; Morley et al., 2016, 2017) and 4 min averaged measurements of THEMIS solid state telescope (SST) (Angelopoulos et al., 2008), that have a 3 s spin resolution. We use CXD electron fluxes evaluated at five energies ([120, 210, 300, 425, 600] keV), as provided in the v1.09 GPS energetic particle data product archived by NOAA (see Data Availability Statement). These energies lie within the range of CXD's Low Energy Particle (LEP) sensor (Tuszewski et al., 2004) and are obtained by flux forward modeling and cross-calibrated with Van Allen Probes (Mauk et al., 2013) measurements as described by Morley et al. (2016). THEMIS SST measurements of fluxes were interpolated into these five energies.

The definition of a conjunction event includes requirements of MLT difference between THEMIS and GPS below 2 hr and L-shell difference (calculated using the T96 model, Tsyganenko, 1995 and TS04, Tsyganenko & Sitnov, 2005 model) below 1. Note that we used two independent data sets of GPS/THEMIS conjugations calculated with two magnetic field models to check how uncertainties of such conjugations impact the final coefficients for equatorial GPS fluxes. Figure 1a shows examples of THEMIS and GPS orbits in L, MLT plane, and

10.1029/2022JA030724

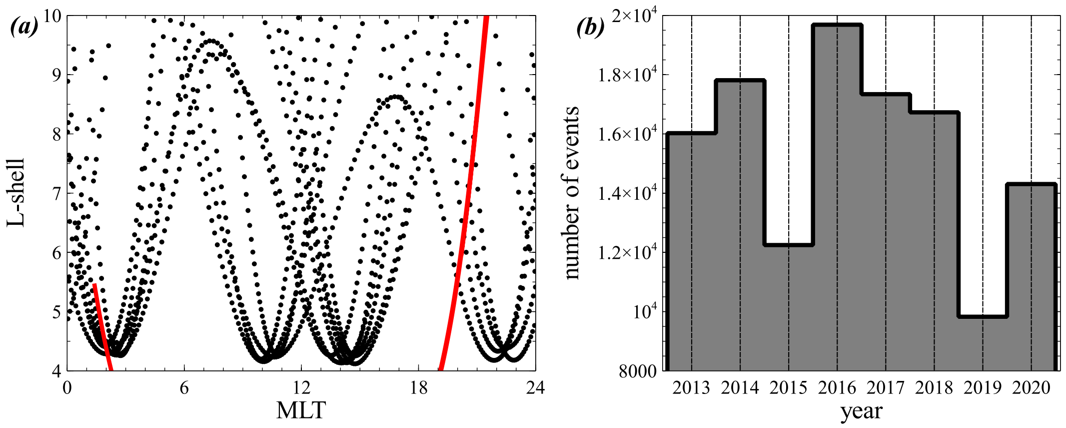

Figure 1. (a) An example of THEMIS (red curve) and several Global Positioning System (GPS) spacecraft (black dots) orbits in the L, MLT plane. (b) The number of THEMIS-GPS conjugation events for different years for (Tsyganenko, 1995) model.

Figure 1b shows total number of such conjunction events between one out of three THEMIS and one out of 20 GPS spacecraft in 2013–2020 (altogether there were ∼124,000 such events).

3. GPS-THEMIS Conjunction Measurements

To compare GPS CXD and THEMIS SST fluxes for a given energy, we bin a L-shell range $L \in [4, 10]$ and we determine a probability distribution $F(J_{GPS}/J_{THEMIS})$ of flux ratio with the normalization of the integral of F to one. Figures 2 and 3 show a set of such 2D distributions in the (L, $\log_{10}(J_{GPS}/J_{THEMIS})$) space for five energies and two magnetic field models used to determine GPS/THEMIS conjugations. The trends of GPS/THEMIS ratio with L are very similar for both data sets. For 120–300 keV, the flux ratio J_{GPS}/J_{THEMIS} decreases with L going from 8 to 5, and for $L < 5$ we can see some weak trend of $J_{GPS}/J_{THEMIS} \to 1$, but this trend is obscured by a large uncertainty of J_{GPS}/J_{THEMIS} due to the THEMIS SST saturation in such low L. For 600 keV, the flux ratio J_{GPS}/J_{THEMIS} increases with L going from 8 to 5, and we have the same problem with high J_{GPS}/J_{THEMIS} spreading for $L < 5$ due to THEMIS SST saturation.

There are at least two main factors contributing to the dependence of J_{GPS}/J_{THEMIS} on L for $L \in [5, 8]$: (a) higher L values mean larger GPS magnetic latitudes and smaller electron fluxes for an anisotropic equatorial electron distribution $J_{THEMIS} \sim \sin^n\alpha_{eq}$ (with $n > 0$ and α_{eq} being the equatorial pitch angle), (b) higher L values correspond to more isotropic electron distributions (due to electron scattering) and $n \to 0$ with an expected weak dependence of J_{GPS} on magnetic latitudes (see pitch angle models of electron fluxes in Gannon et al. (2007), Chen et al. (2014), Shi et al. (2016), and Zhao et al. (2018)). The first effect seems to dominate the dependence of the J_{GPS}/J_{THEMIS} ratio on L-shell for 600 keV electrons with a clear J_{GPS}/J_{THEMIS} decrease for large GPS magnetic latitudes. The second effect seems to dominate the dependence of the J_{GPS}/J_{THEMIS} ratio on L-shell for 120–300 keV, for which the isotropization ($n \to 0$) becomes more significant than the increase of GPS latitudes with L. For 425 keV, electron fluxes these two effects seem to roughly compensate each other and the J_{GPS}/J_{THEMIS} ratio almost does not depend on $L \in [5, 8]$.

For each L-shell bin, we determined the peak of probability distribution $F(J_{GPS}/J_{THEMIS})$ and fit dependence of this peak flux ratio on L as

$$\log_{10}(J_{GPS}/J_{THEMIS}) = a \cdot L + b \tag{1}$$

with energy-dependent coefficients a, b given in Table 1. This fitting is applicable for $L > 5$. The THEMIS SST was not designed to measure high fluxes that are typical for $L < 5$. Fitting (Equation 1) does not show any dependence on MLT of J_{GPS}/J_{THEMIS} because our data set of J_{GPS}/J_{THEMIS} covers all MLT sectors, but we did not find J_{GPS}/J_{THEMIS} dependence on MLT. Figure 4 shows that although the major part of statistics of

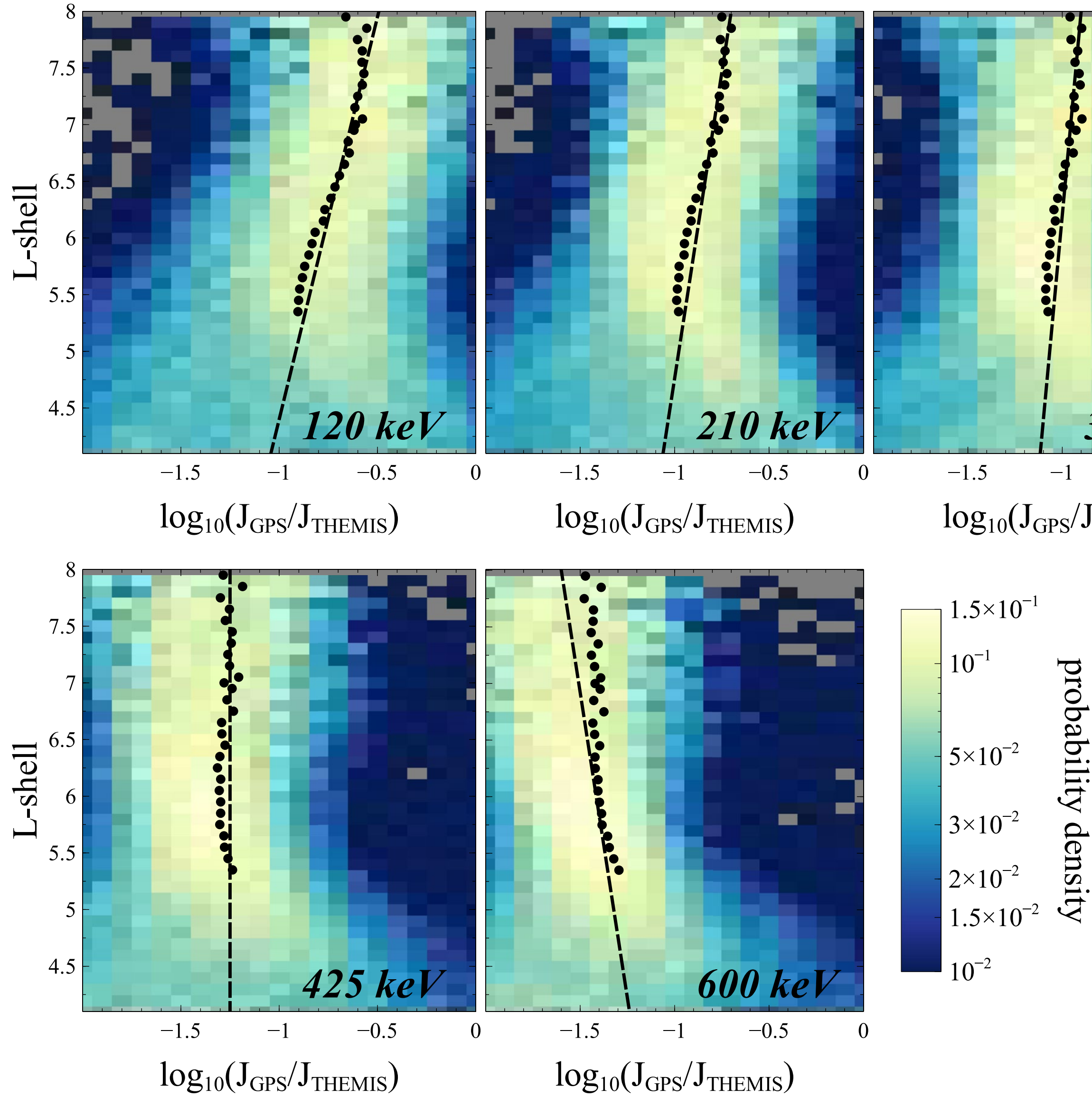

Figure 2. Probability distributions $F(J_{GPS}/J_{THEMIS})$ of the flux ratio for five energies for the data set using (Tsyganenko, 1995) model. For each L-shell bin (i.e., on every row) integral of $F(J_{GPS}/J_{THEMIS})$ is normalized to one, that is, each row shows the conditional probability distribution of $\log(J_{GPS}/J_{THEMIS})$. Thus, the deeper white color indicates the maximum of F on a given row. The same figure, but with a different colormap can be found in Supporting Information S1.

GPS/THEMIS conjunctions are collected around $MLT \in [9, 16]$, we have a good coverage for all MLT bins. Therefore, fitting (Equation 1) should describe the main trend of flux ratio change with L regardless of the MLT value.

4. Projected GPS Fluxes and Comparison With THEMIS Data

To verify our fitting coefficients, we used entire 1 year (2016) of GPS CXD measurements (from all 20 GPS satellites) and projected the measurement fluxes to the equatorial plane according to fitting (Equation 1):

$$J_{GPS}^{eq} = J_{GPS} 10^{-(a_{T96} \cdot L + b_{T96})} \quad (2)$$

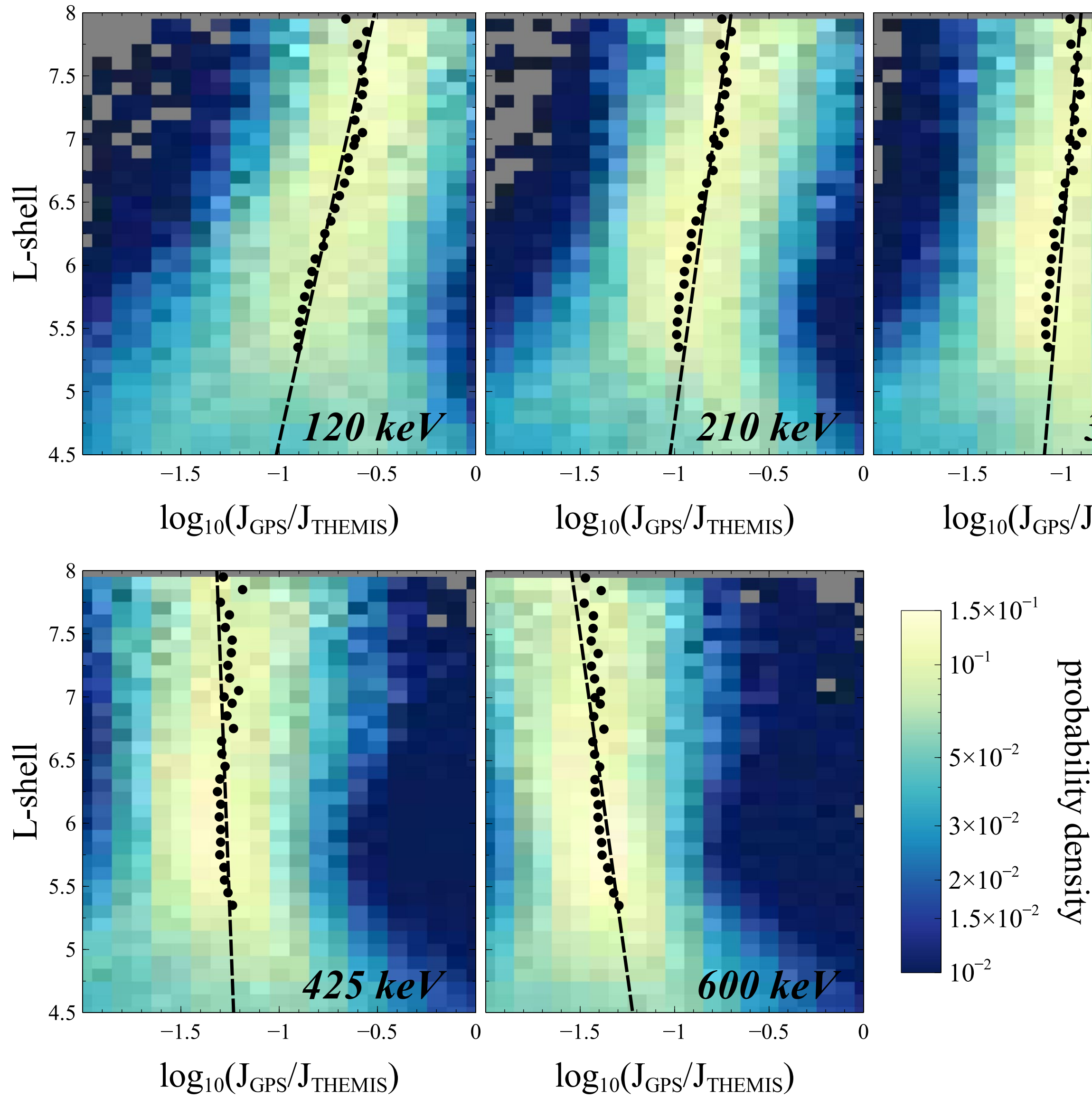

Figure 3. The same as in Figure 2, but for the data set using (Tsyganenko & Sitnov, 2005) model.

Table 1
Coefficients of Fitting $log_{10}(J_{GPS}/J_{THEMIS}) = a \cdot L + b$ for Two Data Sets Compiled With (Tsyganenko, 1995) and (Tsyganenko & Sitnov, 2005) Magnetic Field Models

energy, keV	b_{T96}	a_{T96}	b_{TS04}	a_{TS04}
120	−1.627	0.141	−1.871	0.176
210	−1.444	0.0926	−1.705	0.146
300	−1.344	0.0555	−1.798	0.133
425	−1.25	0.0	1.204	0.006
600	−0.859	−0.093	−1.009	−0.056

Note. These coefficients can be fitted as linear functions of energy: $b_{T96} \approx 0.149 \cdot (E/100\text{ keV}) - 1.799$, $a_{T96} \approx -0.0479 \cdot (E/100\text{ keV}) + 0.1978$, $b_{TS04} \approx 0.353 \cdot (E/100\text{ keV}) - 2.204$, $a_{TS04} \approx -0.052 \cdot (E/100\text{ keV}) + 0.253$.

In other words, J^{eq}_{GPS} is the flux that THEMIS SST is *expected* to measure, had it been located in a conjunction with GPS.

We now compare probability distributions of the projected J^{eq}_{GPS} flux and real THEMIS SST measurements for different energies and L-shells. Figure 5 shows probability distributions (normalized to unity for each L-shell bin) for 120 keV electrons. Projected J^{eq}_{GPS} and J_{THEMIS} fluxes show a similar dependence on L (top panels), whereas probability distributions of these fluxes almost coincide for $L \geq 6$ (bottom panels). For $L < 5.5$, the probability distribution of J_{THEMIS} becomes narrow and fluxes do not exceed a certain limit due to the SST saturation. This explains the difference between GPS and THEMIS fluxes for $L < 5$, where GPS is sufficiently close to the equator to measure the main part of electron pitch angle distribution. Figure 6 is the same as Figure 5, but for the 600 keV energy channel.

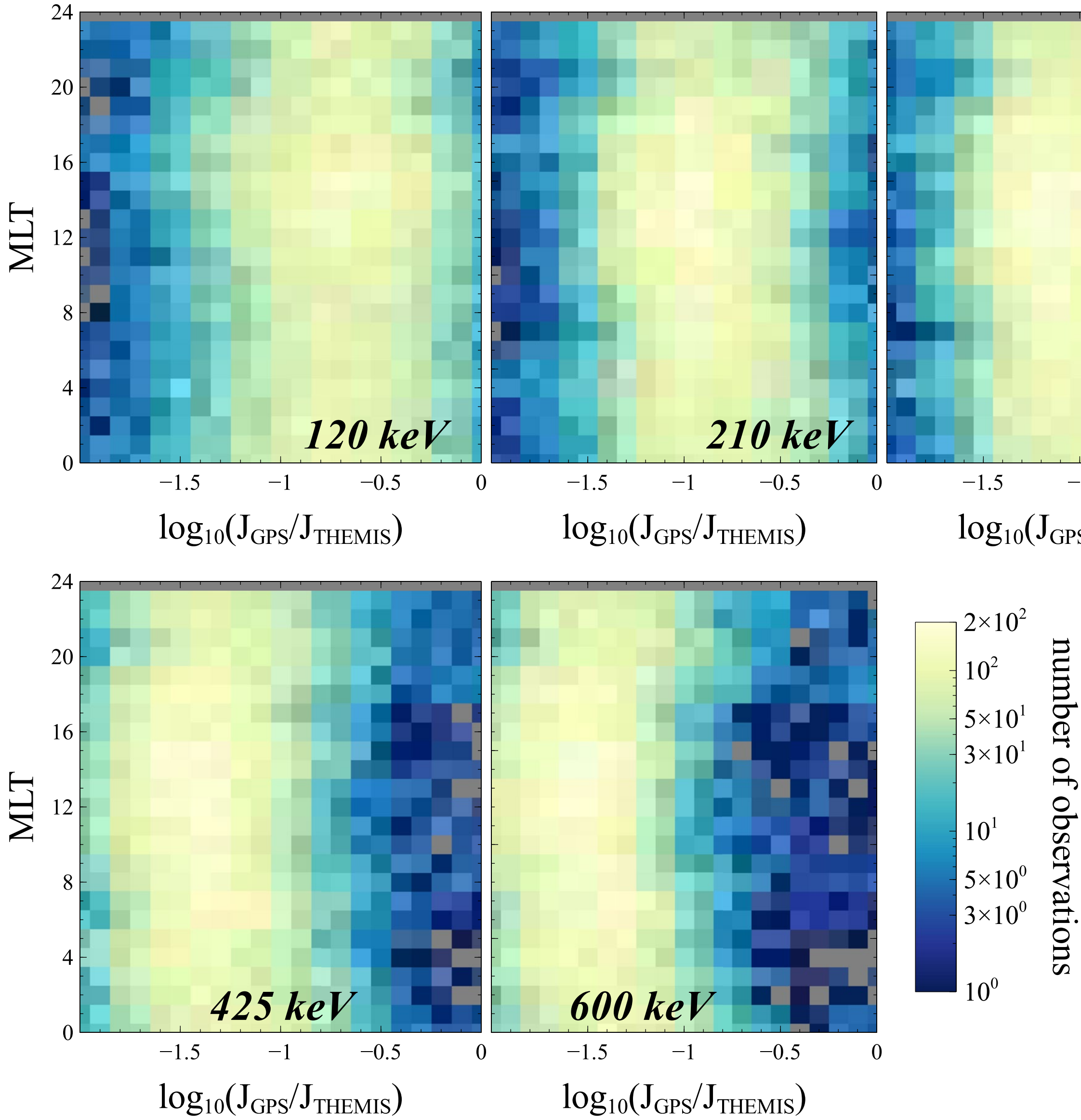

Figure 4. Histograms (number of observations) on the ((J_{GPS}/J_{THEMIS}), *MLT*) plane for five values of energy and $L \in [6, 9]$. The same figure, but with a different colormap can be found in Supporting Information S1.

5. Discussion of Applications of Projected GPS CXD Fluxes

The fittings from Table 1 can be used for projection of GPS CXD fluxes to equatorial values. Taken together, measurements of multiple GPS satellites provide a high-temporal resolution of *L*-shell distributions (Morley et al., 2016; Morley, Friedel, Cayton, et al., 2010). Such projected fluxes can be used for tracing of mesoscale (~hour) dynamics of energetic electron fluxes in the $L \in$ [5, eight] region. Figure 7 shows a comparison of J^{eq}_{GPS} and J_{THEMIS} for ~1 day resolution (full THEMIS orbital period) fluxes for 1 year of observations, whereas Figure 8 shows advantages of a high-temporal resolution J^{eq}_{GPS} for 1 month of measurements. In both figures, the J^{eq}_{GPS}/J_{THEMIS} flux ratio is within [1/3, three] range for $L > 5$ most of the time, which indicates that the projection based on the proposed fitting works well. Figure 8 demonstrates that a high-resolution J^{eq}_{GPS} captures many fine structures of energetic electron flux dynamics: temporally localized ~±1 hr plasma sheet injections shown as flux increase for a wide *L*-shell range and spatially localized $L \in$ [4.5, seven] long-living flux increases (which

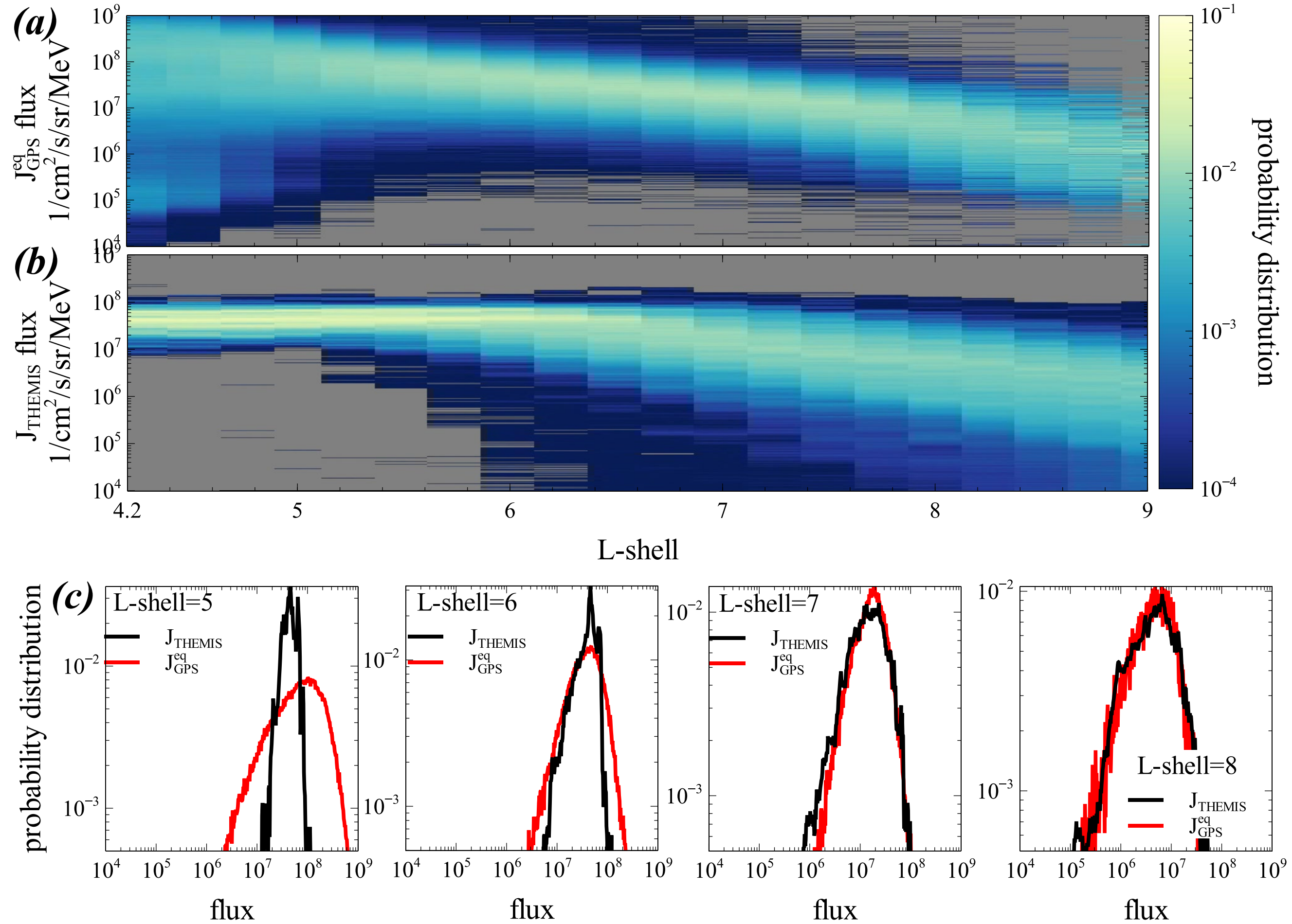

Figure 5. (a, b) Probability distributions of projected Global Positioning System Combined X-ray Dosimeter (GPS CXD) flux J^{eq}_{GPS} and THEMIS SST flux J_{THEMIS} for different *L*-shell bins. For each *L*-shell bin the integral of the probability distribution is normalized to unity. (c) Probability distributions of J^{eq}_{GPS} and J_{THEMIS} for four *L*-shell ranges. Data are presented for the electron energy of 120 keV. The same figure, but with a different colormap can be found in Supporting Information S1.

may be induced by a local acceleration due to the wave-particle resonant interaction, see Green & Kivelson, 2004; Shprits, Subbotin, et al., 2008). Therefore, projected to the equator J^{*}_{GPS} may be useful for tracing the mesoscale dynamics of energetic electrons.

The projected GPS flux data set contains only omnidirectional fluxes J^{eq}_{GPS}. Nevertheless, the high-temporal resolution of *L*-shell flux distributions can be used in investigations that are challenging for data sets collected by equatorial spacecraft with much lower temporal resolution of *L*-shell flux distributions. (a) Combination of the J^{eq}_{GPS} data set (or GPS-based empirical models, e.g., Smirnov et al., 2020) and equatorial (e.g., Van Allen Probes, Mauk et al., 2013; THEMIS, Angelopoulos, 2008; ERG, Miyoshi et al., 2018) spacecraft measurements of electromagnetic waves and energetic electron fluxes can help separating spatial and temporal flux variations. Localized increases/decreases of fluxes associated with the wave activity measured by near-equatorial spacecraft can be compared with high-temporal resolution electron flux J^{eq}_{GPS} distributions along an *L*-shell to separate effects of radially moving injections and local electron acceleration/scattering by waves. (b) Combination of the J^{eq}_{GPS} data set and low-altitude (e.g., POES (Evans & Greer, 2004) and CubeSats (Angelopoulos et al., 2020; Blake & O'Brien, 2016; Johnson et al., 2020)) measurements of electron precipitations can help correlating spatially localized flux variations and electromagnetic wave activity and can supplement existing models projecting low-altitude measurements to the equator (Allison et al., 2018; Claudepierre & O'Brien, 2020). The

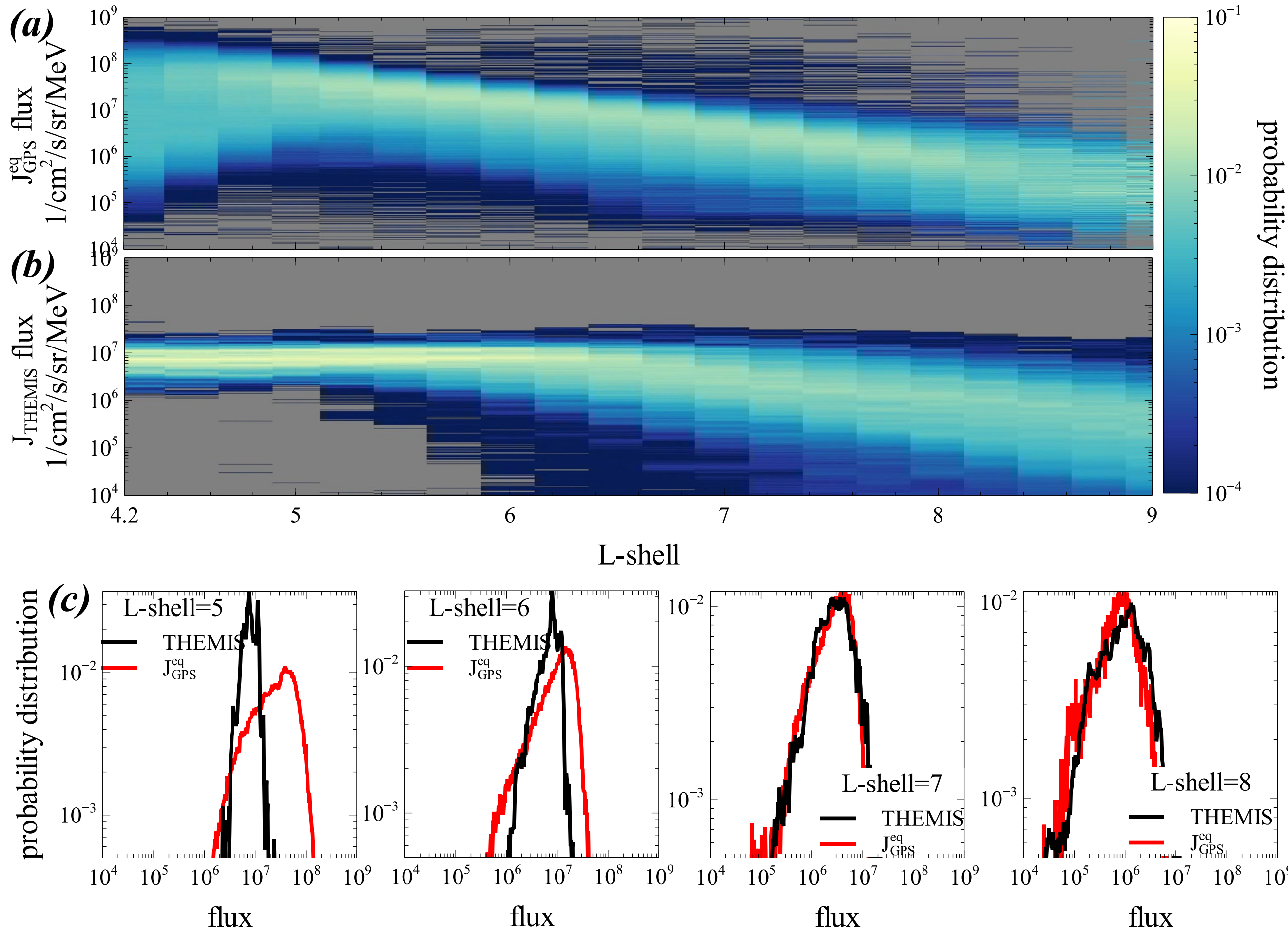

Figure 6. The same as in Figure 5, but for 600 keV. The same figure, but with a different colormap can be found in Supporting Information S1.

enhanced precipitations of ∼30–100 keV electrons measured by low-altitude spacecraft are generally associated with equatorial whistler-mode wave activity (Li et al., 2013; Li, Mourenas, et al., 2014; Ni et al., 2014), whereas precipitations of relativistic electrons are associated with electromagnetic ion cyclotron waves (Blum, Halford, et al., 2015; Capannolo et al., 2019; Y. Zhang, Shi, et al., 2017). Therefore, correlation of intensity of precipitations and high-temporal resolution J^{eq}_{GPS} can reveal the role of whistler-mode waves in localized electron accelerations and help quantifying timescales of such acceleration. (c) Correlation of the J^{eq}_{GPS} data set and ground-based measurements of ultralow-frequency (ULF) waves can help quantifying ULF contribution to the electron radial transport and acceleration and distinguishing this contribution from effects of whistler-mode waves. The high-temporal resolution J^{eq}_{GPS} data set provides almost continuous equatorial flux measurements within given *L*-shell and MLT range. Therefore, such data set can effectively supplement continuous ULF wave measurements by multiple ground-based stations (e.g., Mann et al., 2016). Correlation of J^{eq}_{GPS} variations and ULF wave activity may address the question of different type/characteristics of ULF waves in controlling energetic electron flux dynamics (e.g., Lejosne & Kollmann, 2020).

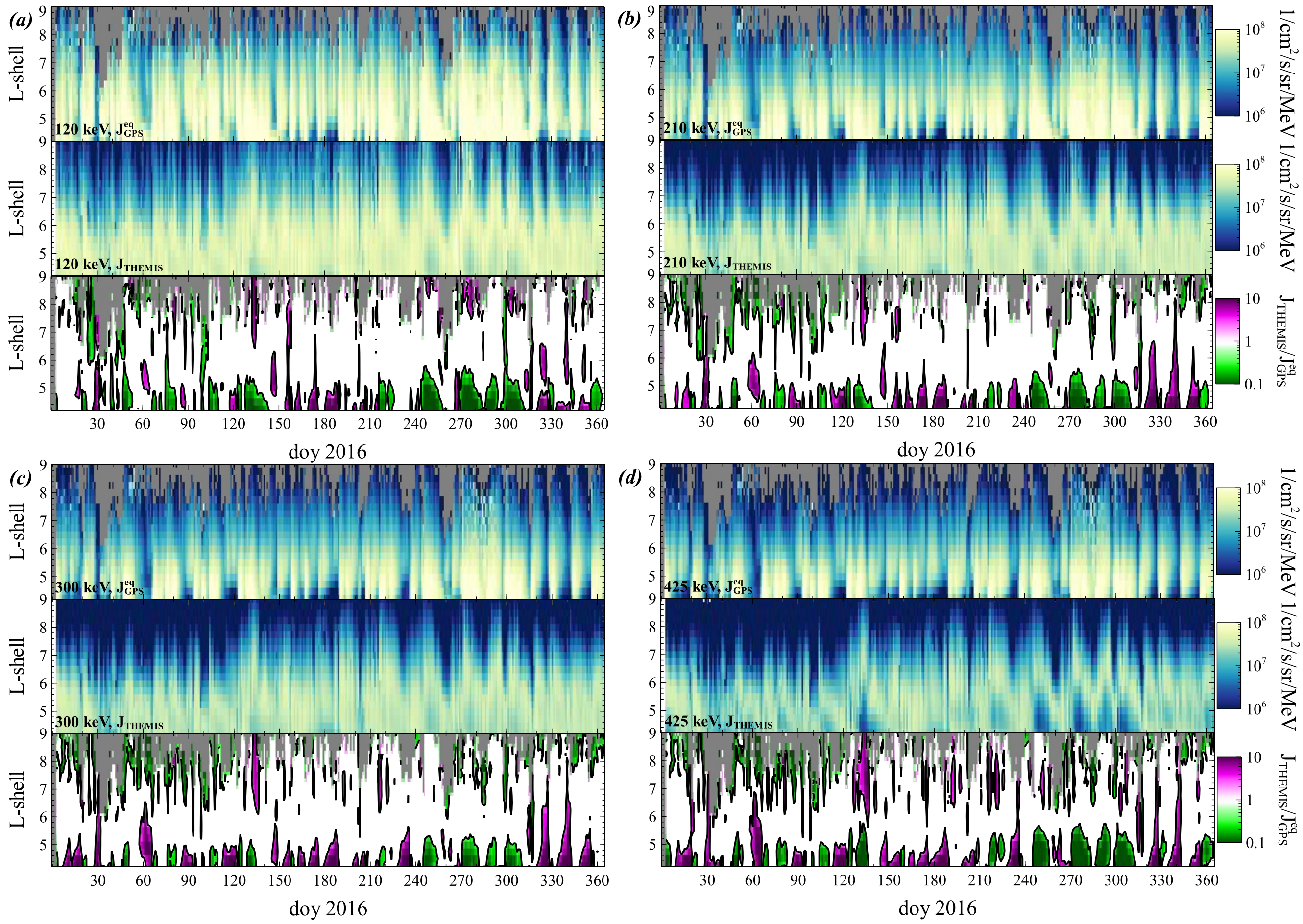

Figure 7. Projected Global Positioning System Combined X-ray Dosimeter (GPS CXD) flux J^{eq}_{GPS} and THEMIS SST flux J_{THEMIS} distributions for four electron energies and 1 year of observations. The time-averaging window is 1 day. In each of four panels, the top plot is J^{eq}_{GPS}, the middle plot is J_{THEMIS}, and at the bottom is the flux ratio J_{THEMIS}/J^{eq}_{GPS}, where the white region is where $J_{THEMIS}/J^{eq}_{GPS} \in [1/3, 3]$. The same figure, but with a different colormap can be found in Supporting Information S1.

6. Conclusions

In this report, we presented results of a comparison of energetic electron flux measurements by near-equatorial THEMIS SST and middle latitude GPS CXD. Using 10 years of THEMIS SST and GPS CXD observations, we compiled a data set of magnetic conjunction (L, MLT) events and determined CXD to SST flux ratio as a function of energy and L-shell. This flux ratio has been fitted as $\log_{10}(J_{GPS}/J_{THEMIS}) = a(E) \cdot L + b(E)$. Obtained fitting allows projection of GPS CXD fluxes to the equatorial plane and such flux projection has been verified for statistics of THEMIS SST and GPS CXD measurements (without restrictions of magnetic conjunction). The projected flux data set provides an opportunity for tracing dynamics of energetic electron flux distributions over L-shell with a high-temporal resolution of ∼1 hr. Moreover, as GPS constellation is active, this projection technique will continue to be applicable into the future as new GPS measurements becomes available.

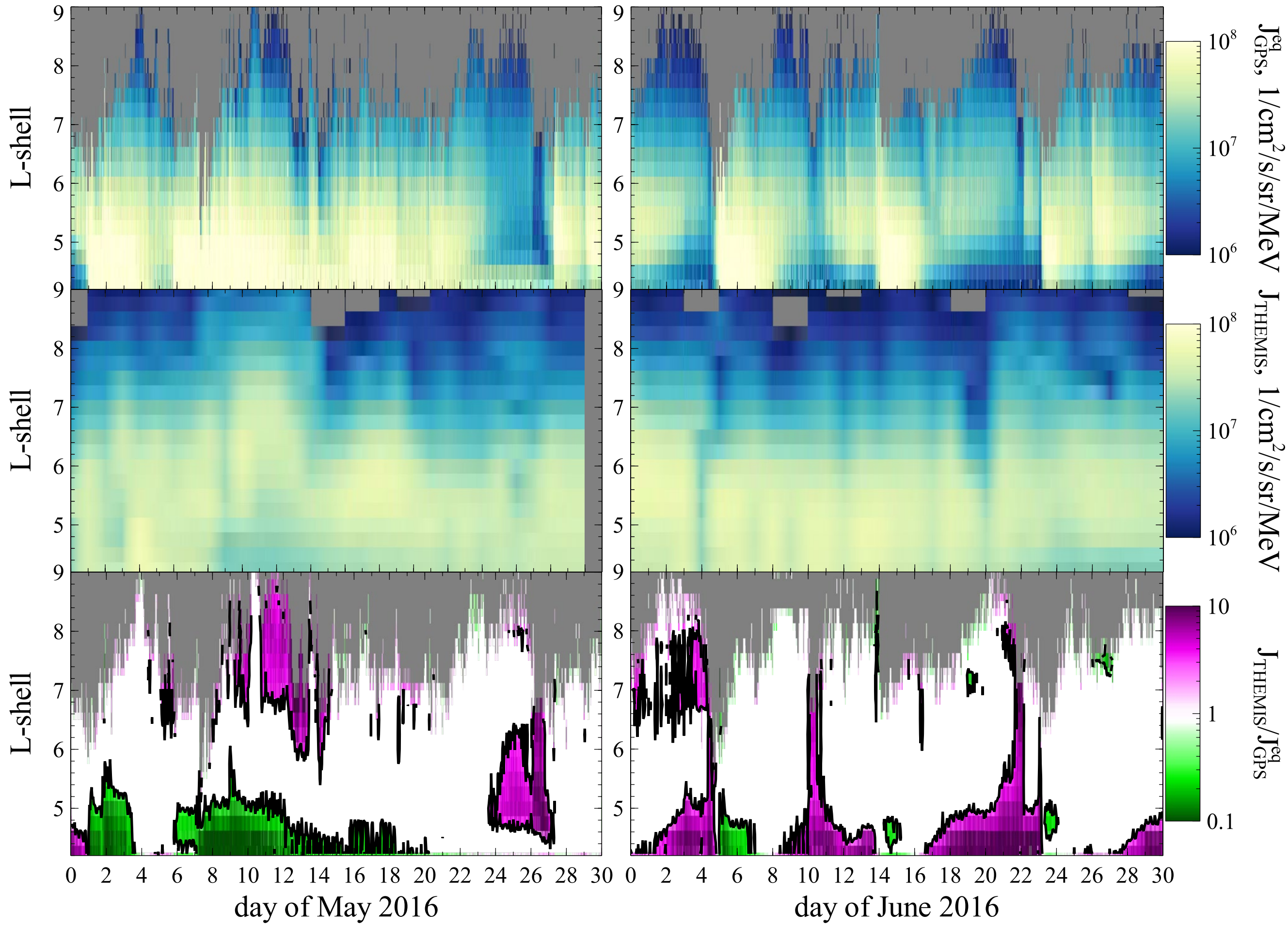

Figure 8. The same format as in Figure 7, but for 210 keV only and 2 months of observations. Time-averaging window for J^{eq}_{GPS} is 1 hr. The same figure, but with a different colormap can be found in Supporting Information S1.

Data Availability Statement

The v1.09 public release of GPS CXD data is available at https://www.ngdc.noaa.gov/stp/space-weather/satellite-data/satellite-systems/gps/data/, and THEMIS SST level 2 data is available at http://themis.ssl.berkeley.edu. THEMIS data T96 model (Tsyganenko, 1995), and TS04 (Tsyganenko & Sitnov, 2005) model access and processing were done using SPEDAS V4.1, see Angelopoulos et al. (2019).

Acknowledgments
We acknowledge support by NASA awards 80NSSC20K1578 (A.V.A., D.L.V.). We thank the GPS CXD team at Los Alamos National Laboratory for design, operation, processing and public release of the GPS energetic charged particle data. Contributions by S.K.M. were performed under the auspices of the US Department of Energy. We acknowledge the support of NASA contract NAS5-02099 for use of data from the THEMIS Mission (A.V.A., V.A.). A.C.K acknowledges support from NASA awards 80NSSC20K1402 and 80NSSC20K1281, and NSF award 2149782.

References

Agapitov, O. V., Artemyev, A. V., Mourenas, D., Mozer, F. S., & Krasnoselskikh, V. (2015). Nonlinear local parallel acceleration of electrons through Landau trapping by oblique whistler mode waves in the outer radiation belt. *Geophysical Research Letters*, *42*, 10140–10149. https://doi.org/10.1002/2015GL066887

Allison, H. J., Horne, R. B., Glauert, S. A., & Del Zanna, G. (2018). Determination of the equatorial electron differential flux from observations at low Earth orbit. *Journal of Geophysical Research: Space Physics*, *123*, 9574–9596. https://doi.org/10.1029/2018JA025786

Allison, H. J., & Shprits, Y. Y. (2020). Local heating of radiation belt electrons to ultra-relativistic energies. *Nature Communications*, *11*, 4533. https://doi.org/10.1038/s41467-020-18053-z

Angelopoulos, V. (2008). The THEMIS mission. *Space Science Reviews*, *141*, 5–34. https://doi.org/10.1007/s11214-008-9336-1

Angelopoulos, V., Cruce, P., Drozdov, A., Grimes, E. W., Hatzigeorgiu, N., King, D. A., et al. (2019). The space physics environment data analysis system (SPEDAS). *Space Science Reviews*, *215*, 9. https://doi.org/10.1007/s11214-018-0576-4

Angelopoulos, V., Sibeck, D., Carlson, C. W., McFadden, J. P., Larson, D., Lin, R. P., et al. (2008). First results from the THEMIS mission. *Space Science Reviews*, *141*, 453–476. https://doi.org/10.1007/s11214-008-9378-4

Angelopoulos, V., Tsai, E., Bingley, L., Shaffer, C., Turner, D. L., Runov, A., et al. (2020). The ELFIN mission. *Space Science Reviews*, *216*(5), 103. https://doi.org/10.1007/s11214-020-00721-7

Birn, J., Thomsen, M. F., Borovsky, J. E., Reeves, G. D., McComas, D. J., Belian, R. D., & Hesse, M. (1998). Substorm electron injections: Geosynchronous observations and test particle simulations. *Journal of Geophysical Research*, *103*, 9235–9248. https://doi.org/10.1029/97JA02635

Birn, J., Thomsen, M. F., & Hesse, M. (2004). Electron acceleration in the dynamic magnetotail: Test particle orbits in three-dimensional magnetohydrodynamic simulation fields. *Physics of Plasmas*, *11*, 1825–1833. https://doi.org/10.1063/1.1704641

Blake, J. B., & O'Brien, T. P. (2016). Observations of small-scale latitudinal structure in energetic electron precipitation. *Journal of Geophysical Research: Space Physics*, *121*, 3031–3035. https://doi.org/10.1002/2015JA021815

Blum, L. W., Halford, A., Millan, R., Bonnell, J. W., Goldstein, J., Usanova, M., et al. (2015). Observations of coincident EMIC wave activity and duskside energetic electron precipitation on 18–19 January 2013. *Geophysical Research Letters*, *42*, 5727–5735. https://doi.org/10.1002/2015GL065245

Blum, L. W., Li, X., & Denton, M. (2015). Rapid MeV electron precipitation as observed by SAMPEX/HILT during high-speed stream-driven storms. *Journal of Geophysical Research: Space Physics*, *120*, 3783–3794. https://doi.org/10.1002/2014JA020633

Boynton, R. J., Mourenas, D., & Balikhin, M. A. (2017). Electron flux dropouts at L ∼ 4.2 from global positioning system satellites: Occurrences, magnitudes, and main driving factors. *Journal of Geophysical Research: Space Physics*, *122*, 11428–11441. https://doi.org/10.1002/2017JA024523

Capannolo, L., Li, W., Ma, Q., Shen, X. C., Zhang, X. J., Redmon, R. J., et al. (2019). Energetic electron precipitation: Multievent analysis of its spatial extent during EMIC wave activity. *Journal of Geophysical Research: Space Physics*, *124*, 2466–2483. https://doi.org/10.1029/2018JA026291

Capannolo, L., Li, W., Ma, Q., Zhang, X.-J., Redmon, R. J., Rodriguez, J. V., et al. (2018). Understanding the driver of energetic electron precipitation using coordinated multisatellite measurements. *Geophysical Research Letters*, *45*, 6755–6765. https://doi.org/10.1029/2018GL078604

Carver, M., Morley, S. K., & Stricklan, A. (2020). GPS Constellation energetic particle measurements. In *IEEE aerospace conference* (pp. 1–10). IEEE. https://doi.org/10.1109/AERO47225.2020.9172652

Chen, Y., Friedel, R. H. W., Henderson, M. G., Claudepierre, S. G., Morley, S. K., & Spence, H. E. (2014). Repad: An empirical model of pitch angle distributions for energetic electrons in the Earth's outer radiation belt. *Journal of Geophysical Research: Space Physics*, *119*, 1693–1708. https://doi.org/10.1002/2013JA019431

Chen, Y., Reeves, G. D., & Friedel, R. H. W. (2007). The energization of relativistic electrons in the outer Van Allen radiation belt. *Nature Physics*, *3*, 614–617. https://doi.org/10.1038/nphys655

Claudepierre, S. G., Ma, Q., Bortnik, J., O'Brien, T. P., Fennell, J. F., & Blake, J. B. (2020a). Empirically estimated electron lifetimes in the Earth's radiation belts: Comparison with theory. *Geophysical Research Letters*, *47*, e2019GL086056. https://doi.org/10.1029/2019GL086056

Claudepierre, S. G., Ma, Q., Bortnik, J., O'Brien, T. P., Fennell, J. F., & Blake, J. B. (2020b). Empirically estimated electron lifetimes in the Earth's radiation belts: Van Allen probe observations. *Geophysical Research Letters*, *47*, e2019GL086053. https://doi.org/10.1029/2019GL086053

Claudepierre, S. G., & O'Brien, T. P. (2020). Specifying high-altitude electrons using low-altitude LEO systems: The SHELLS model. *Space Weather*, *18*, e2019SW002402. https://doi.org/10.1029/2019SW002402

Distel, J. R., Blair, S. G., Cayton, T. E., Dingler, R. D., Guyker, F., Ingraham, J. C., et al. (1999). *The combined X-ray dosimeter cxd on gps block iir satellites* (Tech. Rep. LA-UR-99-2280). Los Alamos Nat. Lab.

Elkington, S. R., Wiltberger, M., Chan, A. A., & Baker, D. N. (2004). Physical models of the geospace radiation environment. *Journal of Atmospheric and Solar-Terrestrial Physics*, *66*(15–16), 1371–1387. https://doi.org/10.1016/j.jastp.2004.03.023

Evans, D. S., & Greer, M. S. (2004). *Polar orbiting environmental satellite space environment monitor-2: Instrument description and archive data documentation*. U.S. Dept. of Commerce, National Oceanic and Atmospheric Administration, Oceanic and Atmospheric Research Laboratories, Space Environment Center.

Foster, J. C., Erickson, P. J., Baker, D. N., Claudepierre, S. G., Kletzing, C. A., Kurth, W., et al. (2014). Prompt energization of relativistic and highly relativistic electrons during a substorm interval: Van Allen Probes observations. *Geophysical Research Letters*, *41*, 20–25. https://doi.org/10.1002/2013GL058438

Gabrielse, C., Angelopoulos, V., Runov, A., & Turner, D. L. (2012). The effects of transient, localized electric fields on equatorial electron acceleration and transport toward the inner magnetosphere. *Journal of Geophysical Research*, *117*, A10213. https://doi.org/10.1029/2012JA017873

Gabrielse, C., Angelopoulos, V., Runov, A., & Turner, D. L. (2014). Statistical characteristics of particle injections throughout the equatorial magnetotail. *Journal of Geophysical Research: Space Physics*, *119*, 2512–2535. https://doi.org/10.1002/2013JA019638

Gabrielse, C., Spanswick, E., Artemyev, A., Nishimura, Y., Runov, A., Lyons, L., et al. (2019). Utilizing the heliophysics/geospace system observatory to understand particle injections: Their scale sizes and propagation directions. *Journal of Geophysical Research*, *124*, 5584–5609. https://doi.org/10.1029/2018JA025588

Galperin, I. I., Gladyshev, V. A., Jorjio, N. V., Kovrazhkin, R. A., Sinitsyn, V. M., Cambou, F., et al. (1978). Adiabatic acceleration induced by convection in the plasma sheet. *Journal of Geophysical Research: Space Physics*, *83*, 2567–2573. https://doi.org/10.1029/JA083iA06p02567

Gan, L., Li, W., Ma, Q., Artemyev, A. V., & Albert, J. M. (2020). Unraveling the formation mechanism for the bursts of electron butterfly distributions: Test particle and Quasilinear simulations. *Geophysical Research Letters*, *47*, e2019GL090749. https://doi.org/10.1029/2020GL090749

Gannon, J. L., Li, X., & Heynderickx, D. (2007). Pitch angle distribution analysis of radiation belt electrons based on Combined Release and Radiation Effects Satellite Medium Electrons A data. *Journal of Geophysical Research*, *112*, A05212. https://doi.org/10.1029/2005JA011565

Grach, V. S., Demekhov, A. G., & Larchenko, A. V. (2021). Resonant interaction of relativistic electrons with realistic electromagnetic ion-cyclotron wave packets. *Earth Planets and Space*, *73*(1), 129. https://doi.org/10.1186/s40623-021-01453-w

Green, J. C., & Kivelson, M. G. (2004). Relativistic electrons in the outer radiation belt: Differentiating between acceleration mechanisms. *Journal of Geophysical Research*, *109*, A03213. https://doi.org/10.1029/2003JA010153

Horne, R. B., Thorne, R. M., Glauert, S. A., Albert, J. M., Meredith, N. P., & Anderson, R. R. (2005). Timescale for radiation belt electron acceleration by whistler mode chorus waves. *Journal of Geophysical Research*, *110*, A03225. https://doi.org/10.1029/2004JA010811

Hudson, M. K., Baker, D. N., Goldstein, J., Kress, B. T., Paral, J., Toffoletto, F. R., & Wiltberger, M. (2014). Simulated magnetopause losses and Van Allen Probe flux dropouts. *Geophysical Research Letters*, *41*, 1113–1118. https://doi.org/10.1002/2014GL059222

Hudson, M. K., Elkington, S. R., Lyon, J. G., Goodrich, C. C., & Rosenberg, T. J. (1999). *Simulation of radiation belt dynamics driven by solar wind variations* (Vol. 109, pp. 171–182). American Geophysical Union Geophysical Monograph Series. https://doi.org/10.1029/GM109p0171

Hudson, M. K., Kress, B. T., Mueller, H.-R., Zastrow, J. A., & Bernard Blake, J. (2008). Relationship of the Van Allen radiation belts to solar wind drivers. *Journal of Atmospheric and Solar-Terrestrial Physics*, *70*, 708–729. https://doi.org/10.1016/j.jastp.2007.11.003

Johnson, A. T., Shumko, M., Griffith, B., Klumpar, D. M., Sample, J., Springer, L., et al. (2020). The FIREBIRD-II CubeSat mission: Focused investigations of relativistic electron burst intensity, range, and dynamics. *Review of Scientific Instruments*, *91*(3), 034503. https://doi.org/10.1063/1.5137905

Kersten, T., Horne, R. B., Glauert, S. A., Meredith, N. P., Fraser, B. J., & Grew, R. S. (2014). Electron losses from the radiation belts caused by EMIC waves. *Journal of Geophysical Research: Space Physics*, *119*, 8820–8837. https://doi.org/10.1002/2014JA020366

Le Contel, O., Roux, A., Jacquey, C., Robert, P., Berthomier, M., Chust, T., et al. (2009). Quasi-parallel whistler mode waves observed by THEMIS during near-Earth dipolarizations. *Annales Geophysicae*, *27*, 2259–2275. https://doi.org/10.5194/angeo-27-2259-2009

Lejosne, S., & Kollmann, P. (2020). Radiation belt radial diffusion at Earth and beyond. *Space Science Reviews*, *216*(1), 19. https://doi.org/10.1007/s11214-020-0642-6

Li, W., & Hudson, M. K. (2019). Earth's van allen radiation belts: From discovery to the van allen probes era. *Journal of Geophysical Research: Space Physics*, *124*, 8319–8351. https://doi.org/10.1029/2018JA025940

Li, W., Mourenas, D., Artemyev, A., Agapitov, O., Bortnik, J., Albert, J., et al. (2014). Evidence of stronger pitch angle scattering loss caused by oblique whistler-mode waves as compared with quasi-parallel waves. *Geophysical Research Letters*, *41*, 6063–6070. https://doi.org/10.1002/2014GL061260

Li, W., Ni, B., Thorne, R. M., Bortnik, J., Green, J. C., Kletzing, C. A., et al. (2013). Constructing the global distribution of chorus wave intensity using measurements of electrons by the POES satellites and waves by the Van Allen Probes. *Geophysical Research Letters*, *40*, 4526–4532. https://doi.org/10.1002/grl.50920

Li, W., Thorne, R. M., Ma, Q., Ni, B., Bortnik, J., Baker, D. N., et al. (2014). Radiation belt electron acceleration by chorus waves during the 17 March 2013 storm. *Journal of Geophysical Research: Space Physics*, *119*, 4681–4693. https://doi.org/10.1002/2014JA019945

Lyons, L. R. (1984). Electron energization in the geomagnetic tail current sheet. *Journal of Geophysical Research*, *89*, 5479–5487. https://doi.org/10.1029/JA089iA07p05479

Ma, Q., Li, W., Thorne, R. M., Bortnik, J., Reeves, G. D., Kletzing, C. A., et al. (2016). Characteristic energy range of electron scattering due to plasmaspheric hiss. *Journal of Geophysical Research: Space Physics*, *121*, 11737–11749. https://doi.org/10.1002/2016JA023311

Ma, Q., Li, W., Thorne, R. M., Bortnik, J., Reeves, G. D., Spence, H. E., et al. (2017). Diffusive transport of several hundred keV electrons in the Earth's slot region. *Journal of Geophysical Research: Space Physics*, *122*, 10235–10246. https://doi.org/10.1002/2017JA024452

Mann, I. R., Ozeke, L. G., Murphy, K. R., Claudepierre, S. G., Turner, D. L., Baker, D. N., et al. (2016). Explaining the dynamics of the ultra-relativistic third Van Allen radiation belt. *Nature Physics*, *12*, 978–983. https://doi.org/10.1038/nphys3799

Mauk, B. H., Fox, N. J., Kanekal, S. G., Kessel, R. L., Sibeck, D. G., & Ukhorskiy, A. (2013). Science objectives and rationale for the radiation belt storm Probes mission. *Space Science Reviews*, *179*, 3–27. https://doi.org/10.1007/s11214-012-9908-y

Millan, R. M., & Baker, D. N. (2012). Acceleration of particles to high energies in Earth's radiation belts. *Space Science Reviews*, *173*, 103–131. https://doi.org/10.1007/s11214-012-9941-x

Millan, R. M., & Thorne, R. M. (2007). Review of radiation belt relativistic electron losses. *Journal of Atmospheric and Solar-Terrestrial Physics*, *69*, 362–377. https://doi.org/10.1016/j.jastp.2006.06.019

Miyoshi, Y., Shinohara, I., Takashima, T., Asamura, K., Higashio, N., Mitani, T., et al. (2018). Geospace exploration project ERG. *Earth Planets and Space*, *70*(1), 101. https://doi.org/10.1186/s40623-018-0862-0

Morley, S. K., Friedel, R. H. W., Cayton, T. E., & Noveroske, E. (2010). A rapid, global and prolonged electron radiation belt dropout observed with the Global Positioning System constellation. *Geophysical Research Letters*, *37*, L06102. https://doi.org/10.1029/2010GL042772

Morley, S. K., Friedel, R. H. W., Spanswick, E. L., Reeves, G. D., Steinberg, J. T., Koller, J., et al. (2010). Dropouts of the outer electron radiation belt in response to solar wind stream interfaces: Global positioning system observations. *Royal Society of London Proceedings Series A*, *466*, 3329–3350. https://doi.org/10.1098/rspa.2010.0078

Morley, S. K., Sullivan, J. P., Carver, M. R., Kippen, R. M., Friedel, R. H. W., Reeves, G. D., & Henderson, M. G. (2017). Energetic particle data from the global Positioning System constellation. *Space Weather*, *15*, 283–289. https://doi.org/10.1002/2017SW001604

Morley, S. K., Sullivan, J. P., Henderson, M. G., Blake, J. B., & Baker, D. N. (2016). The global positioning system constellation as a space weather monitor: Comparison of electron measurements with Van Allen Probes data. *Space Weather*, *14*, 76–92. https://doi.org/10.1002/2015SW001339

Mourenas, D., Artemyev, A. V., Zhang, X. J., Angelopoulos, V., Tsai, E., & Wilkins, C. (2021). Electron lifetimes and diffusion rates inferred from ELFIN measurements at low altitude: First results. *Journal of Geophysical Research*, *126*, e2021JA029757. https://doi.org/10.1029/2021JA029757

Mourenas, D., Ma, Q., Artemyev, A. V., & Li, W. (2017). Scaling laws for the inner structure of the radiation belts. *Geophysical Research Letters*, *44*, 3009–3018. https://doi.org/10.1002/2017GL072987

Ni, B., Bortnik, J., Thorne, R. M., Ma, Q., & Chen, L. (2013). Resonant scattering and resultant pitch angle evolution of relativistic electrons by plasmaspheric hiss. *Journal of Geophysical Research*, *118*, 7740–7751. https://doi.org/10.1002/2013JA019260

Ni, B., Cao, X., Zou, Z., Zhou, C., Gu, X., Bortnik, J., et al. (2015). Resonant scattering of outer zone relativistic electrons by multiband EMIC waves and resultant electron loss time scales. *Journal of Geophysical Research: Space Physics*, *120*, 7357–7373. https://doi.org/10.1002/2015JA021466

Ni, B., Li, W., Thorne, R. M., Bortnik, J., Green, J. C., Kletzing, C. A., et al. (2014). A novel technique to construct the global distribution of whistler mode chorus wave intensity using low-altitude POES electron data. *Journal of Geophysical Research*, *119*, 5685–5699. https://doi.org/10.1002/2014JA019935

Niyazov, R. A., Morley, S. K., Hoover, A. S., & Norman, B. (2021). Gps energetic charged particle data product files (v1.09)(Tech. Rep. LA-UR-21-22607). Retrieved from https://www.ngdc.noaa.gov/stp/space-weather/satellite-data/satellite-systems/gps/readme_v1.09.pdf

Omura, Y., & Zhao, Q. (2013). Relativistic electron microbursts due to nonlinear pitch angle scattering by EMIC triggered emissions. *Journal of Geophysical Research: Space Physics*, *118*, 5008–5020. https://doi.org/10.1002/jgra.50477

Rodger, C. J., Kavanagh, A. J., Clilverd, M. A., & Marple, S. R. (2013). Comparison between POES energetic electron precipitation observations and riometer absorptions: Implications for determining true precipitation fluxes. *Journal of Geophysical Research: Space Physics*, *118*, 7810–7821. https://doi.org/10.1002/2013JA019439

Shi, R., Summers, D., Ni, B., Fennell, J. F., Blake, J. B., Spence, H. E., & Reeves, G. D. (2016). Survey of radiation belt energetic electron pitch angle distributions based on the Van Allen Probes MagEIS measurements. *Journal of Geophysical Research: Space Physics*, *121*, 1078–1090. https://doi.org/10.1002/2015JA021724

Shprits, Y. Y., Drozdov, A. Y., Spasojevic, M., Kellerman, A. C., Usanova, M. E., Engebretson, M. J., et al. (2016). Wave-induced loss of ultra-relativistic electrons in the Van Allen radiation belts. *Nature Communications*, *7*, 12883. https://doi.org/10.1038/ncomms12883

Shprits, Y. Y., Elkington, S. R., Meredith, N. P., & Subbotin, D. A. (2008). Review of modeling of losses and sources of relativistic electrons in the outer radiation belt I: Radial transport. *Journal of Atmospheric and Solar-Terrestrial Physics*, *70*, 1679–1693. https://doi.org/10.1016/j.jastp.2008.06.008

Shprits, Y. Y., Subbotin, D. A., Meredith, N. P., & Elkington, S. R. (2008). Review of modeling of losses and sources of relativistic electrons in the outer radiation belt II: Local acceleration and loss. *Journal of Atmospheric and Solar-Terrestrial Physics*, *70*, 1694–1713. https://doi.org/10.1016/j.jastp.2008.06.014

Shprits, Y. Y., Thorne, R. M., Friedel, R., Reeves, G. D., Fennell, J., Baker, D. N., & Kanekal, S. G. (2006). Outward radial diffusion driven by losses at magnetopause. *Journal of Geophysical Research*, *111*, A11214. https://doi.org/10.1029/2006JA011657

Smirnov, A. G., Berrendorf, M., Shprits, Y. Y., Kronberg, E. A., Allison, H. J., Aseev, N. A., et al. (2020). Medium energy electron flux in Earth's outer radiation belt (MERLIN): A machine learning model. *Space Weather*, *18*, e2020SW002532. https://doi.org/10.1029/2020SW002532

Sorathia, K. A., Ukhorskiy, A. Y., Merkin, V. G., Fennell, J. F., & Claudepierre, S. G. (2018). Modeling the depletion and recovery of the outer radiation belt during a geomagnetic storm: Combined MHD and test particle simulations. *Journal of Geophysical Research: Space Physics*, *123*, 5590–5609. https://doi.org/10.1029/2018JA025506

Tao, X., Thorne, R. M., Li, W., Ni, B., Meredith, N. P., & Horne, R. B. (2011). Evolution of electron pitch angle distributions following injection from the plasma sheet. *Journal of Geophysical Research*, *116*, A04229. https://doi.org/10.1029/2010JA016245

Thorne, R. M., Bortnik, J., Li, W., & Ma, Q. (2021). Wave-particle interactions in the Earth's magnetosphere. In *Magnetospheres in the solar system* (pp. 93–108). American Geophysical Union (AGU). https://doi.org/10.1002/9781119815624.ch6

Thorne, R. M., Li, W., Ni, B., Ma, Q., Bortnik, J., Chen, L., et al. (2013). Rapid local acceleration of relativistic radiation-belt electrons by magnetospheric chorus. *Nature*, *504*, 411–414. https://doi.org/10.1038/nature12889

Tsyganenko, N. A. (1995). Modeling the Earth's magnetospheric magnetic field confined within a realistic magnetopause. *Journal of Geophysical Research*, *100*, 5599–5612. https://doi.org/10.1029/94JA03193

Tsyganenko, N. A., & Sitnov, M. I. (2005). Modeling the dynamics of the inner magnetosphere during strong geomagnetic storms. *Journal of Geophysical Research*, *110*, A03208. https://doi.org/10.1029/2004JA010798

Turner, D. L., Angelopoulos, V., Li, W., Hartinger, M. D., Usanova, M., Mann, I. R., et al. (2013). On the storm-time evolution of relativistic electron phase space density in Earth's outer radiation belt. *Journal of Geophysical Research: Space Physics*, *118*, 2196–2212. https://doi.org/10.1002/jgra.50151

Turner, D. L., Fennell, J. F., Blake, J. B., Clemmons, J. H., Mauk, B. H., Cohen, I. J., et al. (2016). Energy limits of electron acceleration in the plasma sheet during substorms: A case study with the magnetospheric multiscale (mms) mission. *Geophysical Research Letters*, *43*, 7785–7794. https://doi.org/10.1002/2016GL069691

Turner, D. L., O'Brien, T. P., Fennell, J. F., Claudepierre, S. G., Blake, J. B., Kilpua, E., & Hietala, H. (2015). The effects of geomagnetic storms on electrons in Earth's radiation belts. *Geophysical Research Letters*, *42*, 9176–9184. https://doi.org/10.1002/2015GL064747

Turner, D. L., Shprits, Y., Hartinger, M., & Angelopoulos, V. (2012). Explaining sudden losses of outer radiation belt electrons during geomagnetic storms. *Nature Physics*, *8*, 208–212. https://doi.org/10.1038/nphys2185

Tuszewski, M., Cayton, T. E., Ingraham, J. C., & Kippen, R. M. (2004). Bremsstrahlung effects in energetic particle detectors. *Space Weather*, *2*, S10S01. https://doi.org/10.1029/2003SW000057

Zhang, K., Li, X., Schiller, Q., Gerhardt, D., Zhao, H., & Millan, R. (2017). Detailed characteristics of radiation belt electrons revealed by CSSWE/REPTile measurements: Geomagnetic activity response and precipitation observation. *Journal of Geophysical Research: Space Physics*, *122*, 8434–8445. https://doi.org/10.1002/2017JA024309

Zhang, X., Angelopoulos, V., Artemyev, A. V., & Liu, J. (2018). Whistler and electron firehose instability control of electron distributions in and around dipolarizing flux bundles. *Geophysical Research Letters*, *45*, 9380–9389. https://doi.org/10.1029/2018GL079613

Zhang, Y., Ni, B., Xiang, Z., Zhang, X., Zhang, X., Gu, X., et al. (2018). Inter-satellite calibration of FengYun 3 medium energy electron fluxes with POES electron measurements. *Advances in Space Research*, *61*(9), 2290–2300. https://doi.org/10.1016/j.asr.2018.02.017

Zhang, Y., Shi, R., Ni, B., Gu, X., Zhang, X., Zuo, P., et al. (2017). Inferring electromagnetic ion cyclotron wave intensity from low altitude POES proton flux measurements: A detailed case study with conjugate van allen Probes observations. *Advances in Space Research*, *59*(6), 1568–1576. https://doi.org/10.1016/j.asr.2016.12.035

Zhao, H., Friedel, R. H. W., Chen, Y., Reeves, G. D., Baker, D. N., Li, X., et al. (2018). An empirical model of radiation belt electron pitch angle distributions based on van allen Probes measurements. *Journal of Geophysical Research: Space Physics*, *123*, 3493–3511. https://doi.org/10.1029/2018JA025277